Journal of Power Sources 201 (2012) 121–127

Contents lists available at SciVerse ScienceDirect

Journal of Power Sources

journal homepage: www.elsevier.com/locate/jpowsour

Electrochemical study on co-doped ceria–carbonate composite electrolyte

Rizwan Raza[a,b,*], Haiying Qin[a], Liangdong Fan[a], Kaori Takeda[c], Minoru Mizuhata[c], Bin Zhu[a]

[a] Department of Energy Technology, Royal Institute of Technology (KTH), 10044 Stockholm, Sweden
[b] Department of Physics, COMSATS Institute of Information Technology, 54000 Lahore, Pakistan
[c] Department of Chemical Science and Engineering, Graduate School of Engineering, Kobe University, 1-1 Rokkodai-cho, Nada, Kobe 657-8501, Japan

ARTICLE INFO

Article history:
Received 2 August 2011
Received in revised form 18 October 2011
Accepted 31 October 2011
Available online 6 November 2011

Keywords:
Calcium carbonate
Sodium carbonate
Co-doping
Two phase composite
Ionic conductivity

ABSTRACT

A co-doped ceria–carbonate ($Ce_{0.8}Sm_{0.2-x}Ca_xO_{2-\delta}$–$Na_2CO_3$) has been synthesized by a co-precipitation method. The detailed electrochemical characterizations (e.g. impedance spectra, polarization curve and IV curves) of this composite material are reported and discussed. The two phase nanocomposite electrolytes with carbonate coated on the co-doped ceria displays dual (H^+/O^{2-}) ion conduction at low temperature (300–600 °C) in solid oxide fuel cell. The observed remarkable temperature-dependent of conductivity is attributed to the softening/melting of carbonate phase as the physical state of carbonate phase transforms from solid to molten state. Coexistence of various charge carriers, oxide phase composition, and the oxide–carbonate interfacial area are investigated by Raman spectra. The enhancement of conductivity is also discussed by the general mixing rule/percolation theory of composite interfaces. The co-doping with 2nd phase gives a good approach to realize challenges for solid oxide fuel cell.

1. Introduction

Conventional solid oxide fuel cells (SOFCs) based on yttria stabilized zirconia operate at high temperatures (>750 °C) which cause material and operational problems as well as the cost issue. Decreasing the operating temperature is a main stream for current R&D of SOFC [1–4]. Most efforts have gone into thin-film technologies to develop intermediate temperature SOFC (600–800 °C) [2,3].

A number of new electrolytes for reducing the operating temperatures of SOFC have been developed, such as fluorite structured ion-doped ceria [5,6], perovskite type oxides [7], proton conducting ceramics [8,9], O^{2-} conducting oxides [10,11] and apatite-type oxides [12]. Boysen et al. [13] proposed new ion conductors CsH_2PO_4 which can operate at low temperature range of 200–400 °C. Also some more co-ion conductors were developed [14,15]. All these electrolytes are single-phase materials focusing on creating structural oxygen vacancies or interstitials (e.g. in apatite-type oxides). However, due to structural limitations, sufficient ionic conductivities (0.1 S cm^{-1}) and performance have not been reached.

Ceria–carbonate composite electrolytes have attracted much attention during the last decade for the low temperature solid oxide fuel cell (LTSOFCs) [16–28]. Such composite electrolytes are considered as a new class of ionic conductors for its high conductivity which occurs via interfaces [27–29] with promising applications for low temperature, 300–600 °C SOFCs.

The ceria–carbonate composite electrolyte in a nanocomposite have a number of advantages, such as super-ionic conductivity of 0.1 S cm^{-1} at 300 °C, fast ionic transport at interfaces, dual (H^+/O^{2-}) conductivity, negligible electronic conduction, interface and thermodynamic stabilities [30,31], compared with conventional mono-phase solid electrolytes. Nano effect and interfaces play major role in enhancing the conductivity of these composite electrolyte materials [16]. Therefore, it has been widely accepted that the enhancement effect of forming the composite is related to creating highly conducting paths along the interfaces between the host and second phase [31,32].

The co-doped ceria–carbonate composite also exhibited high conductivity and performance as reported earlier [26]. Therefore, if we combined these two approaches (co-doped and composite) in preparing electrolytes which might produce much higher conductivity as compare to conventional electrolytes at low temperatures.

In two phase electrolytes, doped ceria is the host phase and the carbonate is the second phase. We have developed a cost-effective co-doping composition which the calcium is a second cation into the samaria doped ceria (SDC) [26]. In order to enhance further the conductivity of the material, carbonate was used as a second phase to form the composite with the co-doped ceria.

Electrochemical impedance spectroscopy (EIS) or AC impedance analysis has attracted tremendous attention in this decade for its numerous applications in electrochemical devices [33,34]. It can be used to determine the interfaces, electrochemical mechanism, reaction kinetics, ion conduction and electrode processes based on

* Corresponding author at: Department of Energy Technology, Royal Institute of Technology (KTH), 10044 Stockholm, Sweden. Tel.: +46 762569336.

0378-7753/$ – see front matter © 2011 Elsevier B.V. All rights reserved.
doi:10.1016/j.jpowsour.2011.10.124

the responses of the ac signals [33–36]. It is regarded as a powerful and accurate tool for electrochemical analysis [37]. Therefore, it is widely used in fuel cells especially in the SOFC to describe the interface and conduction mechanisms as compare to other electrochemical techniques [38].

In this work, electrochemical characterization (e.g. impedance spectra, polarization curve/resistance and IV curves) of composite electrolyte is used for depth insight of its ionics conduction and interface mechanism. The sintering effect of gas atmosphere (air and H_2) and carbonate is also studied by AC impedance technique. The enhancement of conductivity at the interface between the two phase nanocomposites electrolyte is discussed by the general mixing rule (GMR)/percolation theory of the composites.

2. Experimental and methodology

2.1. Synthesis of the co-doped composite electrolyte

Ca/Sm co-doped CeO_2–carbonate composite electrolyte (CSDC–Na_2CO_3) was synthesized by co-precipitation method as reported before [26]. The dried precursors were sintered in a furnace at three different temperatures of 600, 700, 800 °C for 3 h for comparison, and named as sample-1, sample-2 and sample-3.

2.2. Single cell fabrication and performance

The single cell of 1.3 cm diameter was fabricated by dry pressing technique using CSDC–Na_2CO_3 and NiZn oxide as electrodes (anode and cathode) [39]. The cell active area was 0.64 cm^2 with a thickness of 0.08 cm. The pellet was sintered at 650 °C for 30 min. A silver paste was coated on both sides of the pellet as current collector.

The cell performance was measured with a computerized instrument (S12, China). H_2 gas was used as a fuel with a flow rate of 100 ml min^{-1} at 1 atm pressure and ambient air was used as oxidant.

2.3. Raman spectra

The sample was excited by the SHG light of Nd:VYO_4 solid laser at 532 nm. Raman spectra were measured by Horiba T-64000 with triple monochromator of which optical alignment is shown elsewhere [40,41]. Wavenumber was calibrated by Si and CCl_4. Each spectrum was measured at the wavenumber range around the $\nu 1$ of CO_3^{2-} ion (*ca.* 1060–1080 cm^{-1}) from 808 to 1377 cm^{-1} by CCD detector with 2048 × 512 channels. Data was collected by Jobin-Yvon Spectra Link at 2047 points of CCD elements.

2.4. Electrochemical analysis and conductivity measurement

A pellet of pure composite electrolyte CSDC–Na_2CO_3 was prepared with thickness of 0.2 cm and diameter of 1.3 cm for electrochemical and conductivity measurements. The silver paste was used as current collector in all measurements. The two probe AC impedance was performed by implementing Versa STAT 4 (Princeton Applied Research, USA) in hydrogen and air atmosphere. In order to study the polarization effect in the cell, AC impedance spectrum measurements of the fuel cell under open circuit voltage (OCV) and after operation condition were performed. For collecting EIS data, the frequency range was used from 0.01 Hz to 1 MHz under 10 mV. In order to evaluate the measured impedance spectra, the experimental data were fitted by software (ZSimpWin, Princeton Applied Research, USA) with equivalent circuit which contains various impedance elements representing the involved reaction steps and found the LRQ parameters from the equivalent circuit analysis.

The AC conductivity of the material was calculated from the open circuit impedance spectra at high frequency arc intercept and the activation energy of the composite electrolyte was calculated from the following Arrhenius equation.

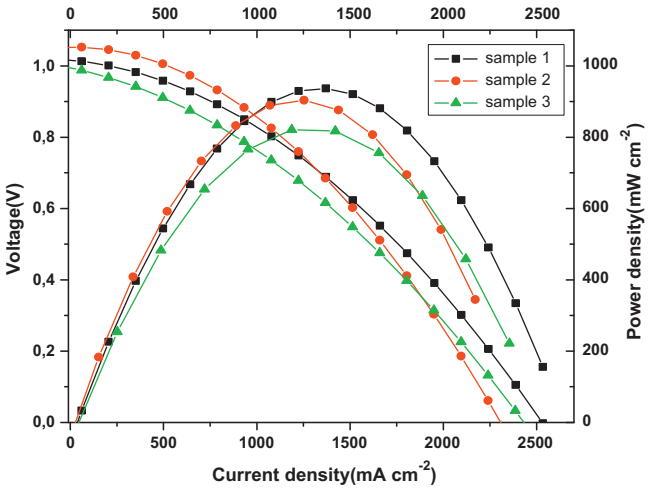

Fig. 1. *I–V*/*I–P* characteristics of single cell of different samples sintered at different temperatures.

3. Results and discussion

3.1. Performance

The oxide/proton ion conductivity of the ceria–carbonate composite electrolyte is in the range of 10^{-1} to 5×10^{-1} S cm^{-1}. The performance of the cell can be estimated with this formula

$$i = \frac{I}{a} = \frac{V}{Ra} = \frac{V}{(\rho L/a)a} = \frac{V\sigma_T}{L} \quad (1)$$

where i is the current density, a is the area of the cell, V is the operating cell voltage, R is the resistance of the electrolyte, ρ is the resistivity and σ_T is the total conductivity (sum of protonic and anion) and L is the thickness of the cell. So, using our experimental results in this equation, $V = 0.6$ V, $\sigma_T = 0.3$–0.5 S cm^{-1}, $L = 0.08$ cm at temperature 500–600 °C. According to these parameters, we can calculate the performance of our cell. Therefore, the current density of our electrolyte supported cell can be calculated to be 2200–2400 mA cm^{-2}, if compatible electrodes are used. We studied the fuel cell performance for three samples sintered at different temperatures. The fuel cell was fabricated using CSDC–Na_2CO_3–NiZn oxide composites for both electrodes and CSDC–Na_2CO_3 as an electrolyte support. It has been observed that the sample 2 sintered at 700 °C have much better performance as compare to other samples, Fig. 1 shows that maximum power densities (P_{max}) of 900, 850 and 800 mW cm^{-2} were achieved at 550 °C. The high cell performance of the low temperature solid oxide fuel cell (LTSOFC) using CSDC–Na_2CO_3 composite as electrolyte exhibits acceptable gas-tightness and negligible electronic conduction.

Since the button cells were sintered at not high temperatures, e.g. conventional co-sintering SOFC pellets needs above 900 °C, while we only use 600 °C. The reason for using lower temperatures to sinter because we have to maintain or maximize interfaces in two-phase composites since the interfaces are the key factors to enhance the ion conductivities which is not same as the conventional structure mechanism. Therefore, there is a limit for sintering to form highly dense button cells in order to maintain or optimize high cell performances. Anyway, there is a conflict aspect to be considered. One way, max interfaces/optimized conductivity, but in the same time, it may get lower dense electrolyte in the button cell; otherwise, higher density, but less interface effect, then low

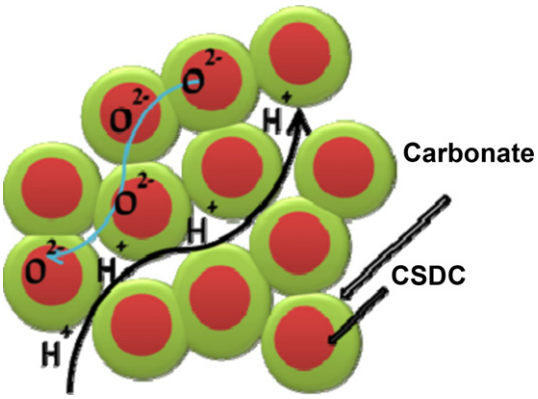

Fig. 2. Schematic figure for co-ion transportaion mechanism.

conductivity and low FC performances, but in the latter, OCV could be higher than the former case.

In addition to that the sealing conditions in laboratory test devices not guarantee from the cell to cell. It may affect the observed OCV values, most importantly; we pay attention to how to enhance power and current outputs from the cells.

The co-ionic conduction in composite electrolytes is considered to be responsible for the enhancement of the total conductivity and performance of our cell. The co-ions mechanism of the composite electrolyte is depicted in a schematic Fig. 2. The protons ions (H^+) passes through the interfaces of the particles and oxygen ions (O^{2-}) are passing through the host particles (doped ceria). The details mechanism is described elsewhere [32]. Due to co-ionic conduction, the LTSOFC has following reaction mechanism.

For H^+/O^{2-} conducting electrolyte case,

at anode:

$$H_2 + O^{2-} \rightarrow H_2O + 2e^- \quad (2)$$

$$H_2 \rightarrow 2H^+ + 2e^- \quad (3)$$

at cathode:

$$(1/2)O_2 + 2e^- \rightarrow O^{2-} \quad (4)$$

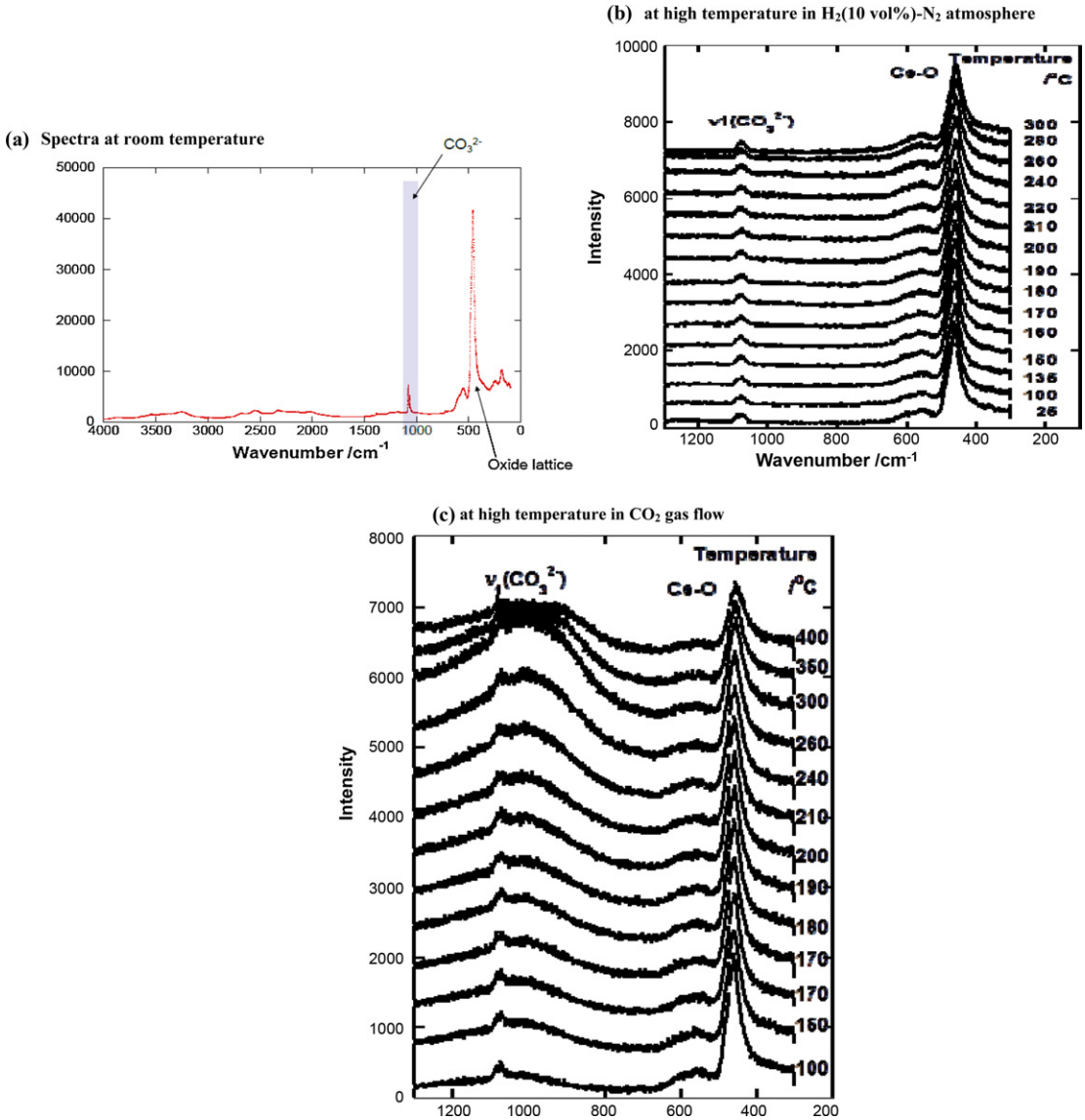

Fig. 3. Raman spectra of CSDC–carbonate composite electrolyte spectra at room temperature at high temperature in H_2(10 vol%)–N_2 atmosphere at high temperature in CO_2 gas flow.

$$(1/2)O_2 + 2H^+ + 2e^- \rightarrow H_2O \quad (5)$$

The overall reaction is:

$$H_2 + (1/2)O_2 \rightarrow H_2O \quad (6)$$

There may be many interesting questions arise concerning the kinetics of these reactions, thus leading to interesting questions concerning the competitive rates, equilibrium constants, as well as dual or hybrid H^+ and O^{2-} conduction/transport in the same time etc. In addition, caused by the dual H^+/O^{2-} transport with H_2O being formed on both the anode and cathode sides, there are also interesting questions regarding depletion and dilution effects in a practical fuel cell. However, these are somehow beyond existing FC scientific knowledge, we will keep continuing effects for a deep study on these issues.

3.2. Raman spectra analysis

The Raman spectra of the CSDC–Na_2CO_3 are shown in Fig. 3. There are two peaks assigned to solid Na_2CO_3 and oxide lattice crystal at room temperature as shown in Fig. 3a. However, above the melting point, the peak is unified into the peak of dissociated carbonate ion in molten salts. These two bands/peaks are ceria lattice at 400 cm^{-1} and carbonate CO_3^{2-} appears at 1100 cm^{-1} but there is no any other bands/peaks was observed [41].

At high temperature, CO_3^{2-} bands are remained even in CSDC composite electrolyte. In H_2 gas atmosphere, CO_3^{2-} bands are united at around 200 °C at which temperature is much lower than conventional melting point of carbonate melts as shown in Fig. 3b. In CO_2 gas; CO_3^{2-} bands increased with increasing temperature as shown in Fig. 3c. It has been observed that the interaction between CeO_2 and CO_3^{2-} are strong. The CeO_2 bands at 400 cm^{-1} are not influenced by heat treatment but CO_3^{2-} bands shown some expansion.

3.3. Electrochemical impedance spectroscopy analysis

The typical AC impedance spectra of the solid ionic conductors show three contributions, one is high frequency arc for bulk, intermediate frequency for grain boundary and low frequency for electrode behavior [25]. The impedance spectra of ceria–carbonate composite electrolyte in air and H_2 are shown in Fig. 4a and b respectively at different temperatures in the range of 400–550 °C. Whereas the low frequency arc is assigned to the conduction of oxide ion. The resistance of the high frequency arc is used to calculate the conductivity *vs.* reciprocal temperature using the electrolyte thickness divided by the active area. The different behavior of this composite electrolyte from simple ceria based electrolytes shows the different ionic process and mechanism but as expected for ceria and carbonate interface. Furthermore, the arc of the material becomes small as temperature increases.

Fig. 5 shows the EIS results for the complete cells with anode, electrolyte and cathode under OCV and after twice fuel cell operations for delivering power outputs. The AC impedance spectra of the cell under OCV at different temperatures are shown in Fig. 5a.

It can be seen that the R_{tot} is decreasing as temperature is increasing from 450 to 550 °C which is a considerable increase in the polarization resistance which was observed in low-frequency range, indicating that slow oxygen diffusion and oxygen reduction might occur in the cathode at 550 °C [39]. The R_1 resistance is assigned to Ohmic. This relatively low ohmic resistance results in higher cell performance. The R_2 and R_3 are assigned to polarization resistances at high frequency (HF) and low frequency (LF) arc. In nanoscale materials, the difference between bulk and grain boundaries is likely to be small and the resultant impedance spectrum may be modeled using a single semi-circle [43].

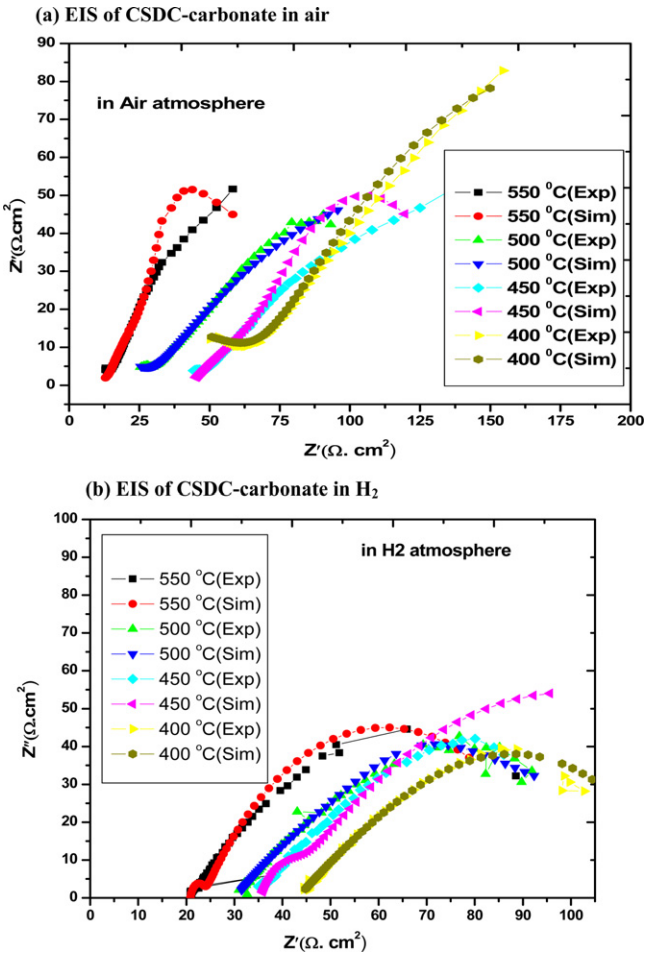

Fig. 4. Electrochemical impedance spectra (EIS) of pure composite electrolyte. (a) EIS spectra in air atmosphere at different temperatures and (b) EIS spectra in H_2 atmosphere at different temperatures.

The interrelation of the different contributions of anode, cathode and electrolyte are illustrated in the form of an equivalent circuit as shown inside Fig 5a and b. The ohmic resistance of electrolyte is known as R_1. The Q is constant phase elements (CPE). The R2Q and R3Q are in series and are due to two arcs in Fig. 5 of cell EIS. R2Q element denotes the high frequency impedance arc and R3Q is due to low frequency impedance arc which is also related to inductance of the connecting leads/cables [42].

The cell was operated twice and analyzed for the impedance spectra at different temperature and the results are shown in Fig. 5b. It can be seen that the overall resistance of the cell decreased with the increasing temperature. However, R_{HF} decreased significantly with the increase in temperature while R_{LF} kept almost the same. The spikes of the arc in the figure indicate that there is electrode effect at high temperature. The experimental data was fitted carefully by an equivalent circuit which shown inside Fig. 5b. The O^{2-} charge transfer is associated with R_{HF} within the electrode dominated the overall electrode kinetic at lower temperature; however, it decreases substantially with the increasing of temperature. This impedance spectrum in a H_2-containing atmosphere suggests a proton conducting mechanism, which has also been observed in SDC–$(Li/Na)_2CO_3$ system [44].

Furthermore, it has been also observe that the overall resistance obtained under OCV condition is larger than that under

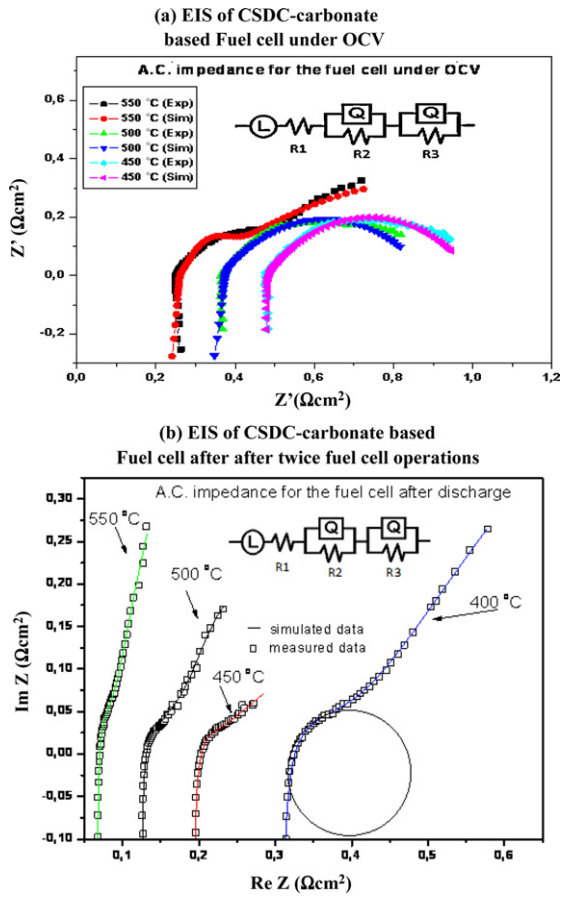

Fig. 5. Electrochemical impedance spectra (EIS) of electrolyte supported cell. (a) EIS spectra of the cell under OCV at different temperatures and (b) EIS spectra of the cell after twice fuel cell operations at different temperatures.

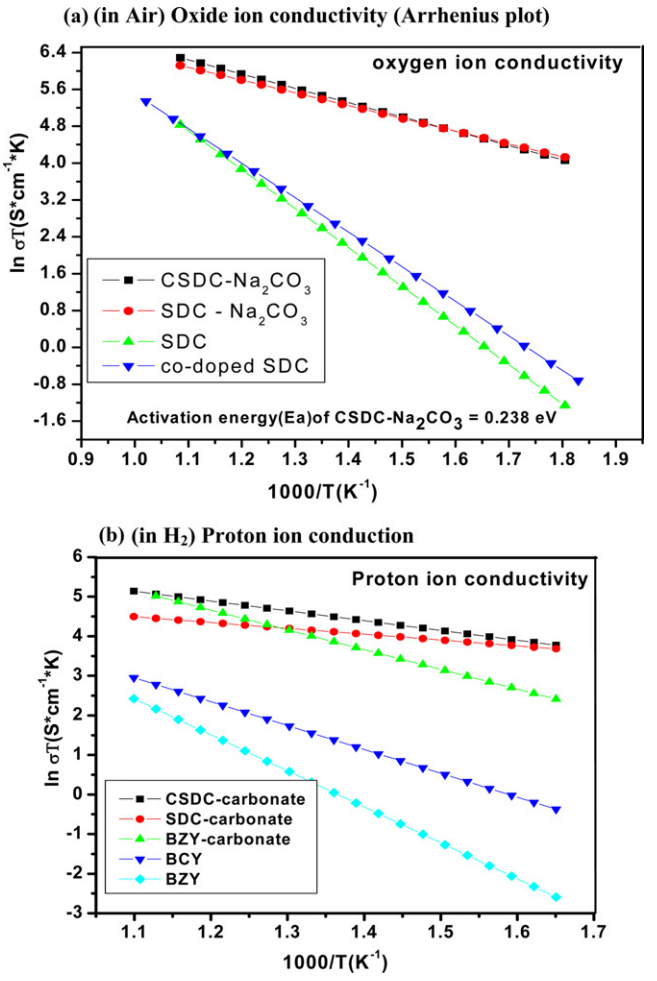

Fig. 6. (a) Oxide ion conductivity of the CSDC–carbonate and comparison with other electrolytes. (b) Proton ion conductivity of the CSDC–carbonate and comparison with other electrolytes.

operating mode. It has been observed in other cells based on different ceria carbonate composite electrolyte due to introducing proton conductivity [45].

3.4. Conductivity (H^+/O^{2-}) of composite electrolyte

The Arrhenius plots of the ionic conductivity for different composite electrolytes have been shown in Fig. 6. Fig. 6a described the oxide ion and Fig. 6b for proton ion conductivity.

It can be seen that the CSDC–Na_2CO_3 exhibits the best ionic conductivity as shown in Fig. 6a. Since there are two effects: one is co-doping and the other is composite, resulting in a interface built between ceria and carbonate. The co-doping can enhance the oxygen ion concentrations and interface between ceria and carbonate facilitates the ions oxide/proton mobilities where the super-ionic conduction pathway takes place. The conductivity of all materials is high at higher temperature due to the conductivity which largely depends on the oxygen/proton ions mobile concentration and has higher mobility at high temperatures.

The activation energy of the CSDC–CSDC–Na_2CO_3 (0.238 eV) is obtained from the Arrhenius relation. It is lower than that of the co-doped ceria electrolyte as reported by Banerjee et al. [33]. This is attributed to the interfaces of the composite material.

Fig. 6b shows proton ion conductivity of composite electrolyte at 500 °C. The proton conduction in bulk oxide and extensive proton exchange and transfer along the interface of the two percolating phases contributes to the enhancement of conductivity.

3.5. Stability of conductivity

Another important parameter, the stability of such nanocomposite electrolytes conductivity was investigates for its major contribution in the performance of the cell. Therefore, we have measured the conductivity for the duration of 21 h in 3 days (7 h per day) at 550 °C as shown in Fig. 7. The conductivity of CSDC–Na_2CO_3 has reduced marginally after 21 h.

3.6. Theoretical calculation on CSDC–Na_2CO_3 conductivity using GMR

The conductivity of the composite materials can be estimated using GMR reported by Uvarov [46]. Therefore, the conductivity of the ceria–carbonate was calculated using Uvarov model. The appropriate form of this rule is expressed as follows,

$$\sigma^{\alpha} = \sigma^{\alpha}_{MX} \cdot (1 - f - f_s) + \sigma^{\alpha}_{s} \cdot f_s + \sigma^{\alpha}_{A} \cdot f \quad (7)$$

Then the generalized equation from Eq. (7) and it can be rewritten as for two phase composite materials;

$$\sigma Ai = [\sigma^{\alpha_i}_{1A} \cdot (1 - f_i - f_{Si}) + 1 \cdot (\sigma_{SA})^{\alpha_i} \cdot f_{Si} + \sigma^{\alpha_i}_{2A} \cdot (f_i)]^{1/\alpha_i} \quad (8)$$

$$\sigma Bi = [\sigma^{\alpha_i}_{1B} \cdot (1 - f_i - f_{Si}) + 1 \cdot (\sigma_{SB})^{\alpha_i} \cdot f_{Si} + \sigma^{\alpha_i}_{2B} \cdot (f_i)]^{1/\alpha_i} \quad (9)$$

Some known parameters are below

$$\alpha_2 = 0.99, \quad i = 0.110, \quad \alpha_1 = 0.3$$

Table 1
The fitted curve results and parameter.

Atmosphere	Experimental results (conductivities of pure components)		Fitted data using mixing rule			
	CSDC ($S\,cm^{-1}$) Phase-1	Carbonate ($S\,cm^{-1}$) Phase-2	Factor-1 ($\alpha 1$)	Factor-2 ($\alpha 2$)	Thickness of the conductive layer, λ ($S\,cm^{-1}$)	Total estimated conductivity, σ_S ($S\,cm^{-1}$)
Air	5×10^{-2}	1×10^{-4}	0.3	0.99	0.2	1.3
H_2	18×10^{-2}	1×10^{-4}	0.3	0.99	0.2	1.5

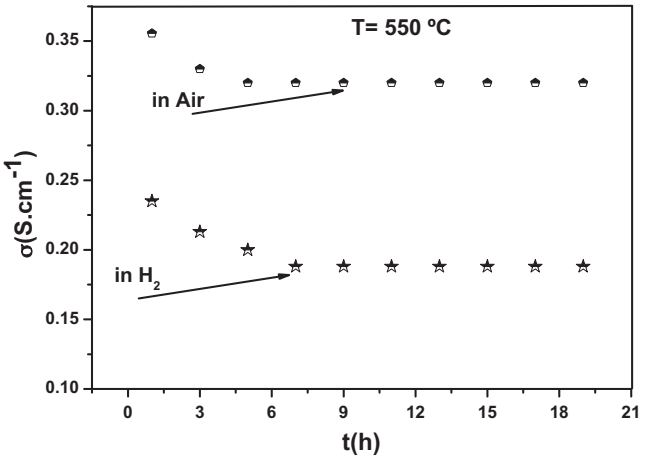

Fig. 7. Stability test for ionic conductivity of the CSDC–carbonate composite electrolyte at 550 °C.

$$f_i = 0.000 + \frac{i}{111}$$

$$\alpha_i = \alpha_1 \cdot (1 - f_i) + \alpha_2 f_i \frac{i}{111}$$

$$f_{Si} = 6 \cdot \lambda \cdot f_i \cdot (1 - f_i)$$

where A is the air atmosphere and B is the H_2 atmosphere σ_S is the composite conductivity, σ_1 is the conductivity of phase 1, σ_2 is the conductivity of phase 2, f is the volume fraction of the second phase

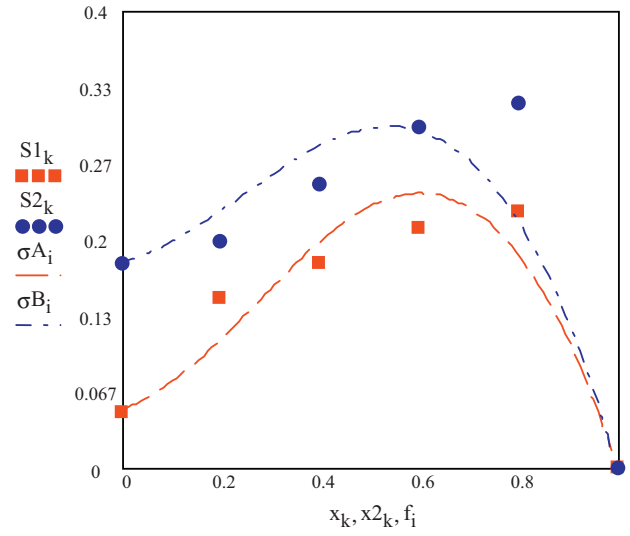

Fig. 8. Composition dependence (volume %) conductivity of a CSDC–carbonate composite and fitting data after using general mixing rule for estimation of conductivity.

of carbonates, and f_s is the volume fraction of high-conducting interface region.

where α_1 and α_2 are the factors, determined by morphology; λ is the thickness of the conductive layer on the interface between the components; f is the volume fraction of high conducting interface regions, σ_S is its conductivity via interface [46].

The conductivities and other parameters are described in Table 1 for both atmospheres;

The experimental conductivity and calculated data was compared in Fig. 8, using Eqs. (8) and (9). There is a good agreement between the qualitatively between the experimental and calculated data through this model. The comparative results from Fig. 8 also agree with the effective medium and percolation theory/models [47]. The fitted curve results and parameter are described in Table 1. It can be seen that the conductivity of the composite electrolyte occurs via highly conducting interfaces because pure carbonate has only a conductivity of $10^{-4}\,S\,cm^{-1}$ at 500 °C [25,44]. It has been observed that this enhanced conductivity is attributed to the parallel connection between two resistances of the ceria and carbonate phases.

4. Conclusion

The ceria-based oxide-ion conductor and carbonate-ion conductor showed impressive conductivity at temperatures close to the carbonates melting temperature for the interfacial and composite effect. The composite effect on the conductivity was also described by GMR which occurs due to super-ionic phase transition at the interphase. The GMR model agreed our experimental results. The highest co-ionic (H^+/O^{2-}) conductivity and performance of the cell 800 mW cm^{-2} was achieved at 550 °C even with a very low activation energy of 0.238 eV.

The excellent results obtained shows that the nanocomposite co-doped ceria–carbonate is a promising electrolyte for LTSOFC and have a pivotal role in the cell performance and stability of SOFC, which explores a new path way for practical SOFCs towards the commercialization. This study contributes to the understanding of the properties of nanocomposite ceria–carbonate electrolyte for LTSOFCs based on the NANOCOFC approach.

Acknowledgements

This research was supported by the Swedish Innovation System (VINNOVA), the Swedish Research Council (VR)/Swedish Agency for International Cooperation and Development (Sida). Professor N.F. Uvarov from Institute of Solid State Chemistry, Novosibirsk, Russian Federation, is also acknowledged to help for calculations. The support of the Higher Education Commission (HEC) is also gratefully acknowledged for their provision of a PhD scholarship.

References

[1] J.B. Goodenough, Nature 404 (1999) 821.
[2] Z.P. Shao, M.H. Sossina, Nature 49 (2004) 170.
[3] R. Doshi, V.L. Richards, J.D. Carter, J. Electrochem. Soc. 146 (1999) 1273.
[4] D.J.L. Brett, A. Atkinson, D. Cumming, Chem. Eng. Sci. 60 (2005) 5649.

[5] E. Perry, T. Tsai, S.A. Barnett, Nature 400 (1999) 649.
[6] B.C.H. Steel, A. Heinzel, Nature 414 (2001) 345.
[7] T. Ishihara, H. Matsuda, Y. Takita, J. Am. Chem. Soc. 116 (1994) 3801.
[8] L. Yang, S. Wang, K. Blinn, M.F. Liu, Z. Liu, Z. Cheng, M.L. Liu, Science 326 (2009) 126.
[9] J.T.S. Irvine, S. Tao, Adv. Mater. 18 (2006) 1581.
[10] P. Lacorre, F. Goutenoire, O. Bohnke, R. Retoux, Y. Laligant, Nature 404 (2000) 856.
[11] J.B. Goodenough, J.E. Ruiz-Díaz, Y.S. Zhen, Solid State Ionics 44 (1990) 21.
[12] Yoshioka, S. Tanase, Solid State Ionics 176 (2005) 31.
[13] D.A. Boysen, T. Uda, C.R.I. Chisholm, S.M. Haile, Science 303 (2004) 68–70.
[14] M. Nagao, A. Takeuchi, P. Heo, T. Hibino, M. Sano, A. Tomita, Electrochem. Solid State Lett. 9 (2006) A105.
[15] X. Chen, C. Wang, E. Payzant, C. Xia, D. Chu, J. Electrochem. Soc. 155 (2008) B1264–B1269.
[16] B. Zhu, Int. J. Energy Res. 30 (2006) 895–901.
[17] L. Zhang, R. Lan, A. Kraft, M. Wang, S. Tao, Electrochem. Commun. 12 (2010) 1589.
[18] W. Liu, Y. Liu, B. Li, T.D. Sparks, X. Wei, W. Pan, Compos. Sci. Technol. 70 (2010) 181–185.
[19] V. Jain, S. Bobade, D. Gulwade, P. Gopalan, Ionics 16 (2010) 487–496.
[20] X. Li, G. Xiao, K. Huang, J. Electrochem. Soc. 158 (2011) B225.
[21] M. Benamira, A. Ringuedé, V. Albin, R.-N. Vannier, L. Hildebrandt, C. Lagergren, M. Cassir, J. Power Sources 196 (2011) 5546–5554.
[22] Y. Ma, X. Wang, S. Li, M.S. Toprak, B. Zhu, M. Muhammed, Adv. Mater. 22 (2010) 1640.
[23] R. Raza, X. Wang, Y. Ma, B. Zhu, Int. J. Hydrogen Energy 5 (2010) 2684.
[24] A.S.V. Ferreira, C.M.C. Soares, Figueiredo, F.M.B. Marques, Int. J. Hydrogen Energy 36 (2011) 3704–3712.
[25] Z. Gao, J.B. Huang, Z.Q. Mao, C. Wang, Z.X. Liu, Int. J. Hydrogen Energy 35 (2010) 731–737.
[26] R. Raza, X. Wang, Y. Ma, B. Zhu, J. Power Sources 195 (2010) 6491.
[27] B. Zhu, J. Power Sources 93 (2001) 82–86.
[28] B. Zhu, J. Power Sources 114 (2003) 1–9.
[29] B. Zhu, X. Liu, P. Zhou, X. Yang, Z. Zhu, W. Zhu, Electrochem. Commun. 3 (2001) 566.
[30] N.F. Uvarov, J. Solid State Electrochem. 15 (2011) 367–389.
[31] X. Wang, Y.R. Ma, Raza. Mamoun, M.B. Zhu, Electrochem. Commun. 10 (2008) 1617–1621.
[32] X. Wang, Y. Ma, S. Li, A. Kashyout, M. Mamoun, B. Zhu, J. Power Sources 196 (2011) 2754–2758.
[33] S. Banerjee, P.S. Devi, D. Topwal, S. Mandal, K. Menon, Adv. Funct. Mater. 17 (2007) 2847–2854.
[34] D.C. Graham, Chem. Rev. 41 (1947) 441–501.
[35] R. Parsons, Modern Aspects of Electrochemistry, in: J.O.M. Bockris, B.E. Conway (Eds.), Butterworths, Kluwer Academic Publisher, London, 1954, p. 103.
[36] P. Delahay, Double Layer and Electrode Kinetics, Wiley-Interscience, New York, 1965.
[37] D.M. Mohilner, Electroanalytical Chemistry, in: A.J. Bard (Ed.), Marcel Dekker publisher, New York, 1966, p. 241.
[38] H.A. Salam, E. El-Shenawy, T. El-Bitar, Int. J. Electrochem. Sci. 1 (2006) 171–180.
[39] R. Raza, Q. Liu, J. Nisar, X. Wang, Y. Ma, B. Zhu, Electrochem. Commun. 13 (2011) 917–920.
[40] M. Mizuhata, T. Ota, S. Deki, Electrochemistry 77 (2009) 721.
[41] M. Mizuhata, T. Ohashi, A. B. Béléké, Int. J. Hydrogen Energy, in press.
[42] C.M. Lapa, F.M.L. Figueiredo, D.P.F. de Souza, L. Song, B. Zhu, F.M.B. Marques, Int. J. Hydrogen Energy 35 (2010) 2953–2957.
[43] M.G. Bellino, D.G. Lamas, N.E. Walsöe de Reca, J. Mater. Chem. 18 (2008) 4537–4542.
[44] X. Wang, Y. Ma, S. Li, A. Kashyout, B. Zhu, M. Muhammed, J. Power Sources 196 (2010) 2754–2758.
[45] L. Fan, C. Wang, M. Chen, J. Di, J. Zheng, B. Zhu, Int. J. Hydrogen Energy 36 (2011) 9987–9993.
[46] N.F. Uvarov, Solid State Ionics 136 (2000) 1667–1672.
[47] T.P. Holme, J. Electrochem. Soc. 157 (2010) B64–B70.